CHAPTER V

ELECTROSPINNING METHOD AS A NEW TECHNIQUE TO CONTROL THE CRYSTAL MORPHOLOGY AND MOLECULAR ORIENTATION OF POLYOXYMETHYLENE NANOFIBER**

*Thontree Kongkhlang[1], Kohji Tashiro[2], Masaya Kotaki[3], Yasushi Kousaka[4], Toshikazu Umemura[4], Daigo Nakaya[5], and Suwabun Chirachanchai[1]**

[1] The Petroleum and Petrochemical College, Chulalongkorn University, Chula Soi 12, Phyathai Road, Pathumwan, Bangkok, Thailand 10330.

[2] Department of Future Industry-oriented Basic Science and Materials, Graduate School of Engineering, Toyota Technological Institute, Tempaku, Nagoya 468-8511, Japan.

[3]Advanced Fibro-science, Kyoto Institute of Technology, Matsugasaki, Sakyo-ku, Kyoto 606-8585, Japan.

[4] Mitsubishi Gas Chemical Company, Mitsubishi Building 5-2, Marunouchi 2-chome, Chiyoda-ku, Tokyo 100-8324, Japan.

[5]Thai Polyacetal Co., Ltd., Padaeng Industrial Estate, 1 Padaeng Rd., Map-Ta-Phut, Rayong, Thailand 21150.

Corresponding author

**The present chapter is from the article submitted to Journal of the American Chemical Society.

ABSTRACT

Electrospinning method is accepted as a convenient technique to produce nanofibers. But, the present work opens a new concept of electrospinning method for controlling the crystal morphology and molecular orientation of nanofibers through the illustration of a case study of polyoxymethylene (POM) nanofibers. Isotropic and anisotropic electrospun POM nanofibers are successfully prepared by using a stationary collector and disc rotating collector. By controlling the voltage and the rotating velocity of the disc rotator, the morphology changes between an extended chain crystal (ECC) and a folded chain crystal (FCC) as clarified by the detailed analysis of X-ray diffraction and polarized infrared spectra of POM nanofibers. Herman's orientation function and dichroic ratio lead us to a schematic conclusion that (i) molecular orientation parallel to fiber axis is observed in both isotropic and anisotropic POM nanofibers, (ii) a single nanofiber consists of an assembly of nanofibril with 60–70 Å in size and tilting at a certain degree, and (iii) the higher the spinning velocity, the smaller the nanofibril under 9/5 helical structure of POM chains. It should be emphasized here the electrospinning method is not anymore a single nanofiber producer but it can work as a new instrument to control the morphology and chain orientation characters of polymer materials, opening a new research field in the polymer science.

Keywords: Electrospinning, polyoxymethylene, molecular orientation, crystal morphology, aligned nanofiber.

1. Introduction

Up to present, electrospinning has been accepted as an efficient technique for the production of polymer fibers with diameters ranging from nano- to micro-scale, providing high surface area to volume ratios, and is of considerable interest for many

applications, such as nanoparticle carrier in controlled release[1], scaffold in tissue engineering[2], wound dressing[3], military wears with chemical and biological resistant protection[4,5], nanofibrous membrane or filter[5], as well as electronic sensors[5,6]. The characteristics of the electrospinning process involve an application of a strong electrostatic field to initiate a polymer jet with a sharp decrease of the jet diameter after its formation.[7] A branching of the jet occurred during the electrospinning process further leads to a decrease in diameter and a time resolution of approximately 0.0125 ms was reported based on the mechanism of the jet formation in electrospinning.[8]

Macroscopically aligned nanofibers by modifying the fiber collecting system to incorporate a rotating mandrel collector[9], a copper wire drum[10], a scanning tip[11], or conductive plates containing an insulating gap[12], have been proposed so far. The production of uniaxially aligned nanofibers of which anisotropic properties are important for use in microelectronics and in a variety of electrical, optical, mechanical, and biomedical applications is considered. However, consideration on the morphology and molecular orientation of polymer chains is very limited.[13,14]

Polyoxymethylene (POM), also known as polyacetal, is an important engineering thermoplastic as well as a crystalline polymer commonly used to replace metals and alloys due to its high tensile strength, impact resistance, stiffness, good dimensional stability, and corrosion resistance. The (9/5) helical structure was first proposed by Tadokoro *et al.* for the molecular conformation of POM to be hexagonal with a unit cell parameters a = 4.47Å and c = 17.39Å.[15] Later, a more accurate (29/16) helical structure was proposed from the layer line intervals by Carazzolo.[16] Recently, Tashiro et al. has refined this crystal structure based on the synchrotron X-Ray and neutron diffraction data. Crystal morphology structure of the crystalline phase is generally classified into two types; an extended-chain crystal (ECC) and a folded-chain or lamellar crystal (FCC), depending on crystallization condition as well as on thermal and mechanical histories.[17] Generally, the properties of POM are significantly influenced by the crystal morphology of the polymer. The typical FCC structure is achieved by crystallizing a dilute POM bromobenzene solution. This generated

hexagon-shaped lamellar crystals with ca. 10 nm thickness, where the molecular chains are folded at the lamellar surface with the stems aligning normal to the surface.[18] The typical ECC structure is achieved through a heterogeneous cationic polymerization of trioxane, giving micron-sized needlelike single crystals where the extended POM molecules align parallel to the needle axis.[19,20] Drawing the fiber is another way to develop ECC-typed POM.[17] The crystal morphology in the melt-grown bulk samples situates in between the above two extremes.[31]

Melt spun POM is an alternative choice to explore new applications; however, the difficulty is about how to prepare POM melt under elevated temperature condition without degradation.[24] In order to avoid this problem, copolymer with small amount of other comonomer is useful as long as the crystallization behavior is not affected seriously.[24]

We succeeded in developing electrospun POM nanofibers of which we proved that inevitable nanopores are generated under TIPS and VIPS mechanisms. However, by controlling the spinning electrical voltage and rotating speed of the disc rotator, we found that (i) the electrospinning easily controls the crystal morphology, and (ii) the morphology is interchangeable. It is important to note that by the careful analysis together with the controlled spinning condition, especially the spinning voltage and the type of the fiber collector including its spinning velocity, we found that we are not only producing inevitable nanoporous nanofiber but we are controlling the crystal morphology and molecular orientation at molecular level. Therefore, herein, we propose that electrospinning is no longer the nanofiber preparation process but it is a novel instrument to control the morphology and chain orientation. This allows us to be possible to investigate and understand how the physical and mechanical properties can be derived under the relationship with the chain morphologies.

Generally, the morphology of extended chain crystals of POM and of highly oriented fibers has been studied using various microscopy techniques[17], electron diffraction technique[23] as well as spectroscopy techniques[17]. The morphological information can be obtained by measuring the small-angle X-ray scattering (SAXS) but

it is quite difficult to measure the SAXS pattern for a thin fiber using an X-ray diffraction of a laboratory level. Rather the infrared spectral measurement is considered to be one of the best methods in the POM case, because the infrared spectra of POM are quite sensitive to the morphology. In the present study, we combine the polarized infrared spectra and the wide-angle X-ray diffraction for the various POM fibers produced by the electrospinning under the drawing equipment to clarify the possibility to control the morphology of electrospun fibers of POM. The present work, thus, shows a case study based on POM nanofiber about the application of a simple electrospinning technique on controlling a complicated morphology of polymer chain packing for the first time.

2. Experimental Section

Materials. Homopolymer of polyoxymethylene was provided by Thai Polyacetal Co. Ltd., Thailand. 1,1,1,3,3,3-hexafluoro-2-propanol (HFIP) was purchased from Nacali Tesque, Inc., Japan. All chemicals were used without further treatment.

Preparation of electrospun POM fibers. Solutions of 5 wt% POM were prepared in HFIP by stirring of the solution at 40°C for 2 hrs. The resulting clear and homogeneous solutions were transferred to a 2.5 mL syringe and electrospun using NANON (MECC Co. Ltd.). The as-spun POM nanofiber was deposited onto a stationary collector whereas the aligned POM nanofiber was deposited onto a rotating metallic disc collector capable of rotating speed up to 1890 m/min. The needle-to-collector distance was fixed at 10 cm, an electrical voltage was 15 kV, and a volumetric flow rate was 0.5 mL/h. Relative humidity was about 30–35%.

Characterizations. Surface morphology of the electrospun POM fiber was observed by a JSM-5200 JEOL scanning electron microscope. The DSC thermograms were measured using a Perkin Elmer Pyris Diamond DSC7 under the flow of N_2 gas at the rate of 20 mL/min and a heating rate of 10°C/min from 25 to 200 °C. The degree of crystallinity

(χ_c) was estimated by assuming that the heat of melting per unit mass of purely crystalline sample is identical to that of melting of a 100% crystalline POM sample (i.e. 317.93 J/g, Iguchi *et al.*).[25] Polarized infrared spectra were measured with a Varian FTS-7000 Fourier-transform infrared spectrometer equipped with a wiregrid polarizer. The resolution power for the IR was 2 cm^{-1}. The X-ray diffraction system was a Rigaku/TTR-III X-ray diffractometer with Cu Kα line as an incident X-ray beam. The X-ray diffraction profiles were measured in a reflection mode in the 2θ range of 10–30° at a scanning rate of 5°/min. The crystallite size was estimated using Scherrer equation, $\langle L \rangle_{hkl} = K\lambda/\beta\cos\theta$, where $\langle L \rangle_{hkl}$ is a crystallite size estimated from the (*hkl*) reflection planes, K is a constant (0.9), λ is the wavelength of incedent X-ray (1.542 nm), β is full width at haft maximum peak intensity (FWHM), and θ is a Bragg angle. The FWHM or β has been corrected for the peak broadening caused by the slit system of the diffractometer in which $\beta^2 = \beta^2_{obs} - \beta^2_m$, where β_{obs} is the FWHM and β_m is the peak broadening due to the slit system. The β_m was estimated from the diffraction peak measured for Si powder sample. Two dimensional wide angle X-ray diffractometer (2D-WAXD) was applied to take the fiber diagrams using an imaging plate system DIP 1000 (MAC Science Co. Japan) with the graphite-monochromatized CuKα line as an incident X-ray beam (λ =1.542 Å). Azimuthal profiles to estimate the degree of orientation of crystallites were obtained from 2D WAXD patterns with the zero angle on the equator and counterclockwise scanning.

3. Results and Discussion

Figure 5.1 shows nanofibers with different diameters and morphologies when the rotating disc collector was applied. Due to the bending instability of the charged jet, an isotropic nanofiber with diameter about 1000 nm was observed when the fiber was collected by a stationary collector (Figure 5.1 (a) and (d)). On the other hand, the aligned POM nanofibers were obtained by adjusting the linear velocity of the disc rotating

collector. Fiber alignment is significantly improved with the velocity (Figure 5.1 (b) and (c)). As the linear velocity increased from 630 m/min to 1890 m/min, the average diameter decreases from 700 nm to 350 nm (Figure 5.1 (e) and (f)). This indicates that the fibers were stretched and aligned toward the rollup direction together with the control in fiber diameter via drawing. In order to understand how the electrospinning process as well as the mechanical drawing affects the crystal morphology and molecular orientation of the nanofiber; polarized FTIR and X-ray diffraction were measured.

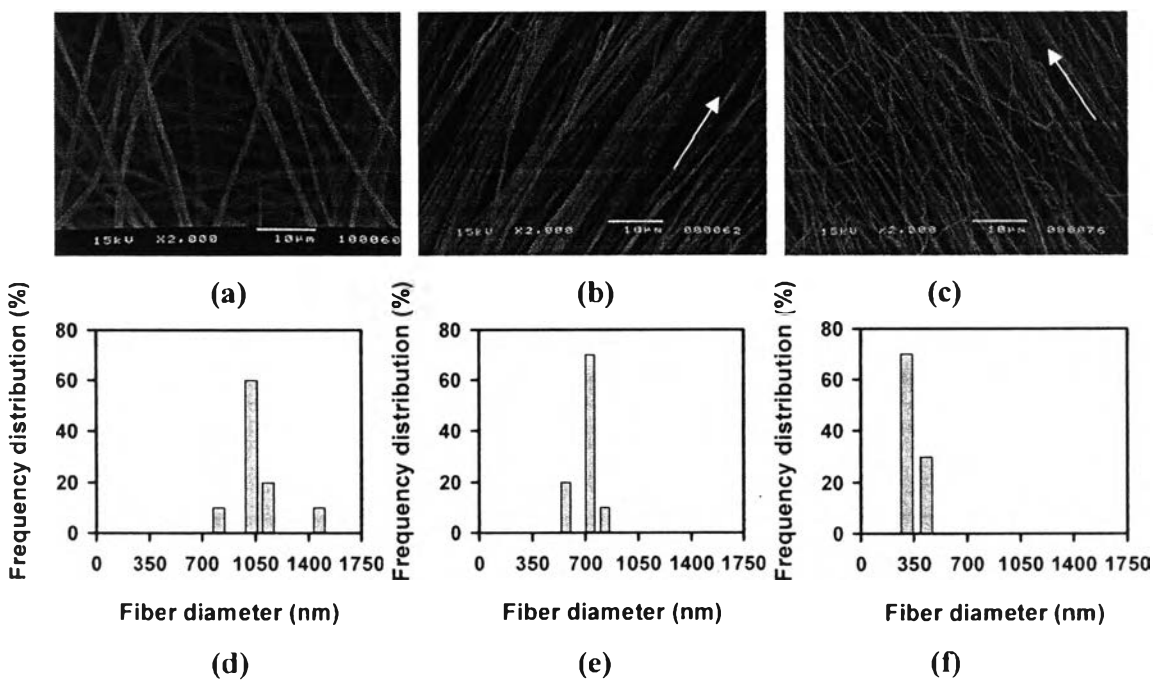

Figure 5.1. Scanning electron micrographs and frequency distribution of electrospun POM nanofiber obtained from using the rotating disc collector with the velocity of (a,d) 0 m/min, (b,e) 630 m/min, and (c,f) 1890 m/min. Arrows indicate drawing direction.

Crystal morphology of electrospun POM nanofiber. Up to present, various reports showed how the vibrational spectrum of the POM with different crystal morphology exhibits specific spectrum patterns which can be used for the characterization of the

morphological structure of the POM samples.[26-29] It should be noted that both ECC and FCC structures give the same X-ray diffraction pattern, but remarkably different IR spectra.[17] The bands due to the A_2 symmetry species, having the transition dipole along the chain axis, show a significant high-frequency shift (as high as 100 cm^{-1}) in the FCC sample as compared with those of the ECC sample (Table 5.1). On the other hand, the infrared- and Raman-active E_1 band (having the transition dipole perpendicular to the chain axis) and the Raman-active and infrared-inactive A_1 and E_2 bands appear at the same frequencies in both FCC and ECC samples.

Table 5.1 FTIR band assignment of polyoxymethylene

Mode	ECC[a]	FCC[a]	Assignment
$E_1(6)$, ⊥	1235, vs	1235, vs	CH_2 rock., δ(OCO), ν_s(COC)
$A_2(3)$, //	1097, vvs	1136, vvs	ν_a(COC), δ(OCO)
$E_1(7)$, ⊥	*f*	1092, vvs	ν_a(COC)
$E_1(8)$, ⊥	935, vvs	935, vvs	ν_s(COC)
$A_2(4)$, //	897, vvs	1002, vvs	ν_a(COC), CH_2 rock.
$E_1(9)$, ⊥	628, s	630, s	δ(OCO)

[a] relative intensity of the infrared band, s: strong, vs: very strong, vvs: very very strong.

The structure of the as-spun POM nanofibers was characterized by FTIR and the result was compared with that acquired from a cast film (prepared from the same solution used for electrospinning). As evidence in Figure 5.2 (b) and Table 5.1, the as-spun POM nanofiber shows the characteristic IR peaks of $A_2(4)$, $E_1(8)$, $E_1(7)$, and $E_1(6)$ bands at the positions corresponding to the ECC morphology. Small shoulder at around 995 cm^{-1} is also observed which is due to the amorphous phase in the system. The cast

film, on the other hand, shows characteristic IR peaks in which $A_2(4)$ band is located at 997 cm^{-1} and $A_2(3)$ band is at 1130 cm^{-1}, corresponding to the band positions expected to the FCC morphology (Figure 5.2 (a)). This implies that the crystal morphology is changed remarkably by electrospinning process. Kobayashi and Sakashita reported that the ECC can be developed upon the sample drawing. For electrospinning process, an electric force is required to overcome both surface tension and viscoelastic force for stretching the fiber. Taking this into our consideration, the stretching during the electrospinning process is substantial for stretching the crystal region to get the ECC morphology.

To confirm that the electrospinning initiates the ECC chain morphology and this packing can be easily changed to FCC, the as-spun POM nanofiber was dissolved in hexafluoro-2-propanol (HFIP) solution followed by re-casting and re-spinning. Figure 5.2 (c) shows important information about the changing from ECC to FCC after recasting. Moreover, the re-spun fiber shows that the ECC is recovered again after re-spinning (Figure 5.2 (d)). This experimental result demonstrates clearly the effectiveness of controlling ECC morphology via electrospinning. It should be emphasized here that the degree of chain orientation in the nanofiber is increased by increasing the rotating speed (see the discussion on Molecular orientation in electrospun POM nanofiber). The important point here is that even though without applying any such a tensile force to the fibers, we can get the nanofibers with highly developed ECC morphology. This is quite important finding in the technical development of the electrospinning method

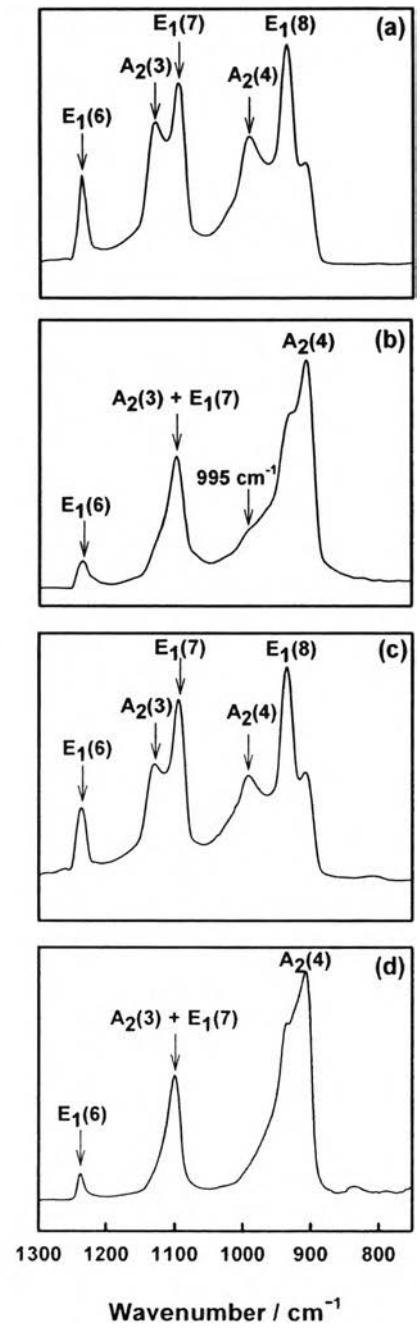

Figure 5.2. FTIR spectra of POM obtained from (a) cast film, (b) as-spun nanofiber, (c) re-cast film, and (d) re-spun nanofiber.

Molecular orientation in electrospun POM nanofiber. Figure 5.3 shows the polarized FTIR spectra of electrospun POM nanofibers which were collected with the disc rotating collector under linear velocity 0, 630, and 1890 m/min. A small portion of the as-spun POM nanofiber is picked up with a special care to avoid force and tension disturbed or destroyed the morphology during sample preparation. Figure 5.3 (a) shows that parallel components of the IR peaks observed at $A_2(4)$ and $A_2(3) + E_1(7)$ bands are significantly higher than those observed for the perpendicular components. This implies that the electrospinning process originally induces the molecular orientation to be parallel to the fiber axis.

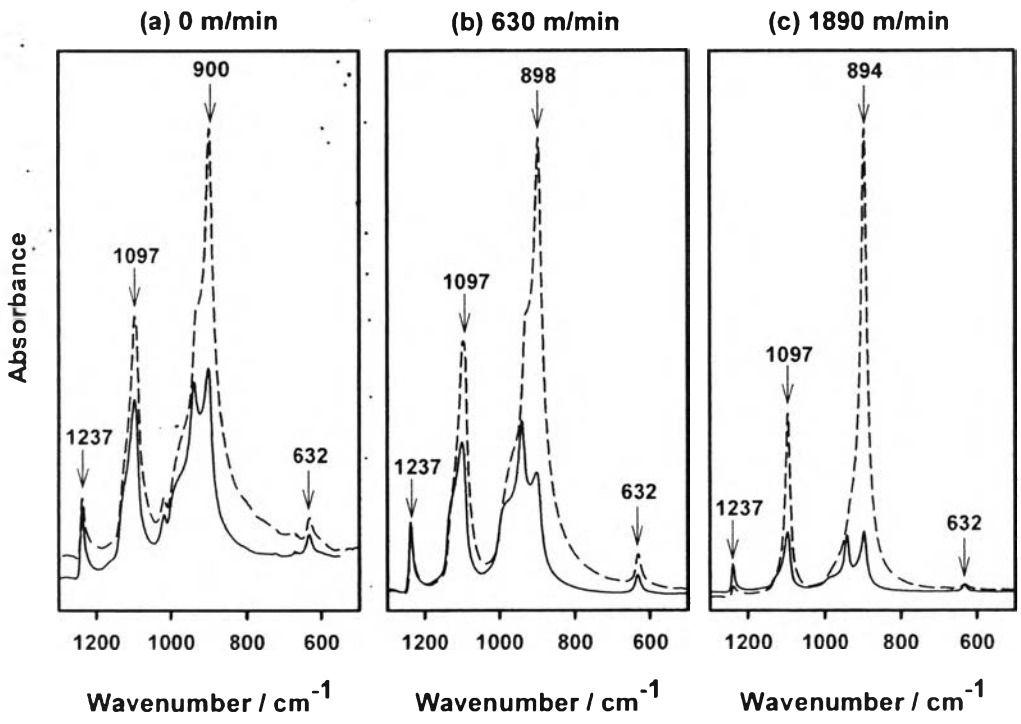

Figure 5.3. Polarized FTIR spectra of electrospun POM nanofiber with linear velocity of (a) 0 m/min, (b) 630 m/min, and (c) 1890 m/min. — Electric vector of an incident IR beam perpendicular to the fiber axis (⊥). – – – Electric vector of an incident IR beam parallel to the fiber axis (//).

A polymer solution is considered to experience two kinds of force during electrospinning; one is a shear force when it flows through a capillary (needle) at a very high rate and the other one is a Columbic force when the jet is elongated and accelerated by the high electric field applied. Both of the shear force and Columbic force possibly initiate synergistically the orientation of the polymer chain. Here, it is expected that an increase in mechanical force during the disc rotating will initiate the increase in molecular orientation of the polymer chain. As our expectation, when the linear velocity of the collector was increased from 0 m/min to 630 m/min and further increased to 1890 m/min, the parallel IR bands of $A_2(4)$ and $A_2(3)+E_1(7)$ bands increase remarkably indicating the better alignment of the polymer chain (Figure 5.3 (b) and (c)). It is important to notice that the frequency position of the $A_2(4)$ band corresponding to the ECC morphology is shifted from 900 cm^{-1} to 898 cm^{-1} and to 894 cm^{-1} as the linear velocity of the disc rotating collector is increased from 0 to 630 and to 1890 m/min, respectively. This implies that an increase in the tensile stress applied to the fiber accelerates the ECC morphology with significant defined structure.

To quantify the degree of uniaxial orientation exhibited by POM molecules, the concept of a dichroic ratio was applied. Dichroic ratio (R) can be calculated by using the formula, $R = A_{//}/A_{\perp}$, where $A_{//}$ is infrared absorbance of parallel component, and $A_{\perp}$ is that of perpendicular component. For a randomly oriented sample, R is equal to 1, and for a perfectly uniaxially oriented sample (all polymer chains are oriented along the fiber axis), R is equal to infinity. The dichroic ratios for the IR bands of the POM nanofibers are summarized in Table 5.2. The infrared peak observed at $A_2(4)$ band (~900 cm^{-1}) corresponds to the ECC whereas that observed at $A_2(3)$ band (~1120 cm^{-1}) corresponds to the FCC. As the linear velocity of the disc rotating collector increases, the ECC component is increased whereas the FCC component is decreased. The FCC peak could not be observed at the highest linear velocity (1890 m/min), resulting in the inexistence of R value. This implies that the polymer chains existing in the crystalline region can be stretched furthermore in the draw direction during the rolling-up process.

Table 5.2 Dichroic ratio ($A_{//}/A_{\perp}$), and thermal properties of POM nanofibers at various rotating disc velocity

Properties	Unit	Linear velocity of disc rotating collector		
		0 (m/min)	630 (m/min)	1890 (m/min)
Dichroic ratio, *R* ($A_2(3)$, ~1120 cm^{-1})	-	0.74	0.67	-
Dichroic ratio, *R* ($A_2(4)$, ~900 cm^{-1})	-	2.15	3.95	7.87
ΔH_m (1^{st} heating)	J/g	174	183	196
ΔH_m (2^{nd} heating)	J/g	168	165	168

As FTIR spectra clearly shows us that the disc rotating speed easily controls the ECC morphology, it is important to find the answer about polymer chain orientation at molecular level. Here, the molecular orientation in electrospun POM nanofibers was further investigated by 2D WAXD. Figure 5.4 shows 2D WAXD patterns of the aligned POM nanofibers collected at the linear velocity of 630 and 1890 m/min. By comparing these two patterns, it is clear that the disc rotating speed enhances orientation of the c-axis into the fiber direction significantly. Comparing the azimuthal profile of the two nanofibers obtained from the different disc rotating speed, it is clear that FWHM of the fiber obtained from the disc rotating speed at 1890 m/min is significantly smaller than that observed at 630 m/min, suggesting the lower degree of the mis-orientation of the polymer chain along the fiber axis (Figure 5.5).

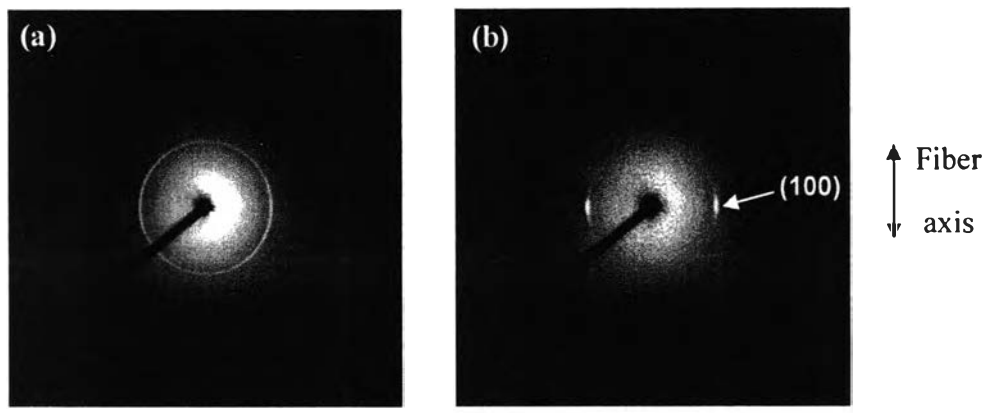

Figure 5.4. Two dimensional (2D) WAXD patterns for the 100 reflection of aligned POM nanofiber at (a) 630 m/min and (b) 1890 m/min.

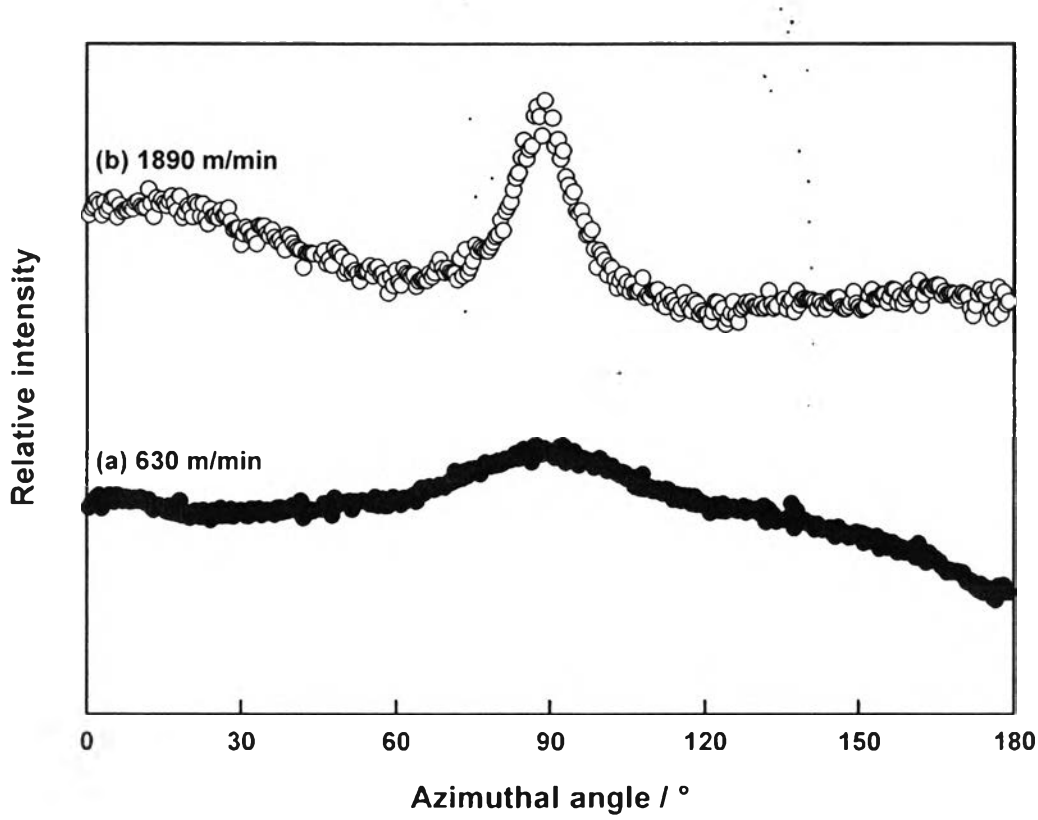

Figure 5.5. Azimuthal-scan profiles for the 100 reflection for aligned POM nanofibers with linear velocity (a) 630 m/min and (b) 1890 m/min.

In order to identify how much the mis-orientation of nanofibril in nanofiber is, Herman's orientation function was applied. Figure 5.6 (a) shows the Herman's orientation function for the various kinds of fibers. Herman's orientation function (*f*) is defined as

$$f = \frac{3\langle \cos^2 \varphi \rangle - 1}{2},$$

where $\cos^2 \varphi$ represents a square averaged of cosine of angle φ between the fiber axis and the crystallographic axis. The value of f is 1 when the polymer chains aligned perfectly parallel to the fiber axis and -0.5 when the polymer chains aligned perfectly perpendicular to the fiber axis. When f is zero, it means for the random orientation. In our case, the calculation of f was simplified by simply calculating the misorientation appeared in azimuthal scan as shown in Figure 5.5. The value of f can be calculated by the following equation:

$$f = \frac{180° - \Delta\varphi_{1/2}}{180°},$$

where $\Delta\varphi_{1/2}$ represents the FWHM of the azimuthally-scanned peak (Figure 5.5). Figure 5.6 (a) shows that the orientation function increases as the linear velocity of the disc rotating collector is increased. Especially, the nanofiber obtained at 1890 m/min gives f = 0.93 which is very close to 1, indicating that the polymer chains are oriented almost parallel to the fiber axis.

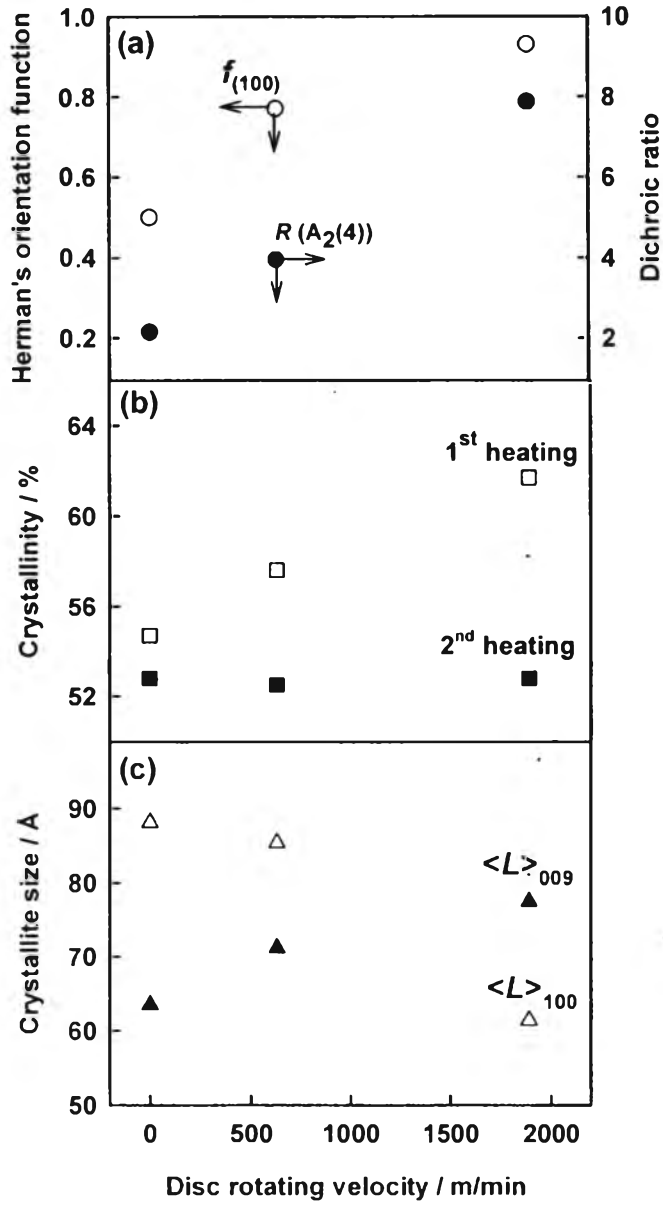

Figure 5.6. (a) Herman's orientation function (○) and dichroic ratio of $A_2(4)$ band at 900 cm^{-1} (●), (b) crystallinity estimated from the enthalpy of melt of the 1st heating (□) and 2nd heating (■), and (c) crystallite size estimated from 100 reflection (Δ) and 009 reflection (▲), as a function of linear velocity of the disc rotating collector.

Degree of crystallinity and crystallite size. Table 5.2 also shows the enthalpy of melt of the as-spun and aligned POM nanofibers. In our case, the enthalpy of melt observed in the first heating (ΔH_m, 1st heating) refers to the degree of crystallinity initiated by the electrospinning process. On the other hand, ΔH_m observed in the second heating refers to the degree of crystallinity after slowly cooling from the melt. The ΔH_m observed in the 1st heating increases gradually as the rotating speed is increased, implying the increase in crystallinity. Besides, it is significantly higher than that observed in the 2nd heating. Figure 5.6 (b) clearly shows the change in crystallinity as an effect of electrospinning process with various rotating disc collector, which confirms how electrospinning process induces the crystallization of POM.

Figure 5.6 (c) shows the change in crystallite size estimated from Scherrer's equation for the 100 and 009 reflections. As the linear velocity of the disc rotating collector increases from 0 m/min to 630 m/min and to 1890 m/min, the $\langle L \rangle_{100}$ decreases from 88.1 Å to 85.4 Å and to 61.4 Å, respectively, whereas the $\langle L \rangle_{009}$ is simultaneously increased from 63.5 Å to 71.2 Å and to 77.5 Å. Up to this point, we may say the following points; (i) the electrospinning method gives the highly oriented ECC crystals with relatively high crystallinity even without any additional tension and (ii) by applying the tensile force during the disc rotation, the degree of orientation and crystallinity are enhanced remarkably. At the same time, the crystallite size along the fiber direction is increased while that in the lateral direction $\langle L \rangle_{100}$ is decreased gradually.

Structure of POM nanofiber. Considering the overall results, the detailed structure of POM nanofiber is speculated with schematic illustration as shown in Figure 5.7. Tadokoro et al. reported the crystal conformation of 9/5 helical structure in the fiber period of 17.39Å.[15] In the case of the electrospun POM nanofiber with disc rotation at 1890 m/min, the $\langle L \rangle_{009}$ for 77.5 Å and $\langle L \rangle_{100}$ for 61.4 Å lead us to a schematic nanofiber with about 40 monomeric units and a bundle of 14 chains arranging along the chain axis in an X-ray coherent domain.

According to the theory by Kobayashi et al., the *R/H* ratio of the crystallite governs the vibrational frequency of the infrared A_2 bands.[17] For example, the

$\langle L\rangle_{100}/\langle L\rangle_{009}$ gives the value 0.8 for the nanofiber obtained by 1890 m/min rotating speed, which should predict the peak position of the A_2 band closer to FCC. This is inconsistent with the actually observed infrared spectral profile, which corresponds to the almost perfect ECC morphology. We speculate this situation in the following way. The infrared-active vibrational mode comes from the aggregation of groups vibrating in-phase. This can be said for both of the chain direction and the lateral direction. The X-ray diffraction occurs from the domain which should consist of the positionally-regular array of the groups. The coherent (or in-phase) size of the "static" and "vibrating" units might be different in some senses. In a single nanofiber, the vibrationally matched domains are aggregated to form the geometrically-coherent region as illustrated in Figure 5.8 (a). Another possibility is the existence of so-called tie chains in between the neighboring crystallites, as proposed by Hama et al.[31] The extended chains can pass through the neighboring crystallites and they form the bundle of small size (Figure 5.8 (b)). These bundles have smaller *R/H* ratio because $H>>R$. These bundles do not contribute to the X-ray diffraction positively but affect the infrared spectral profile remarkably. We need to investigate the relation between the *R/H* ratio estimated by the IR data and the crystallite size by X-ray data in more detail.

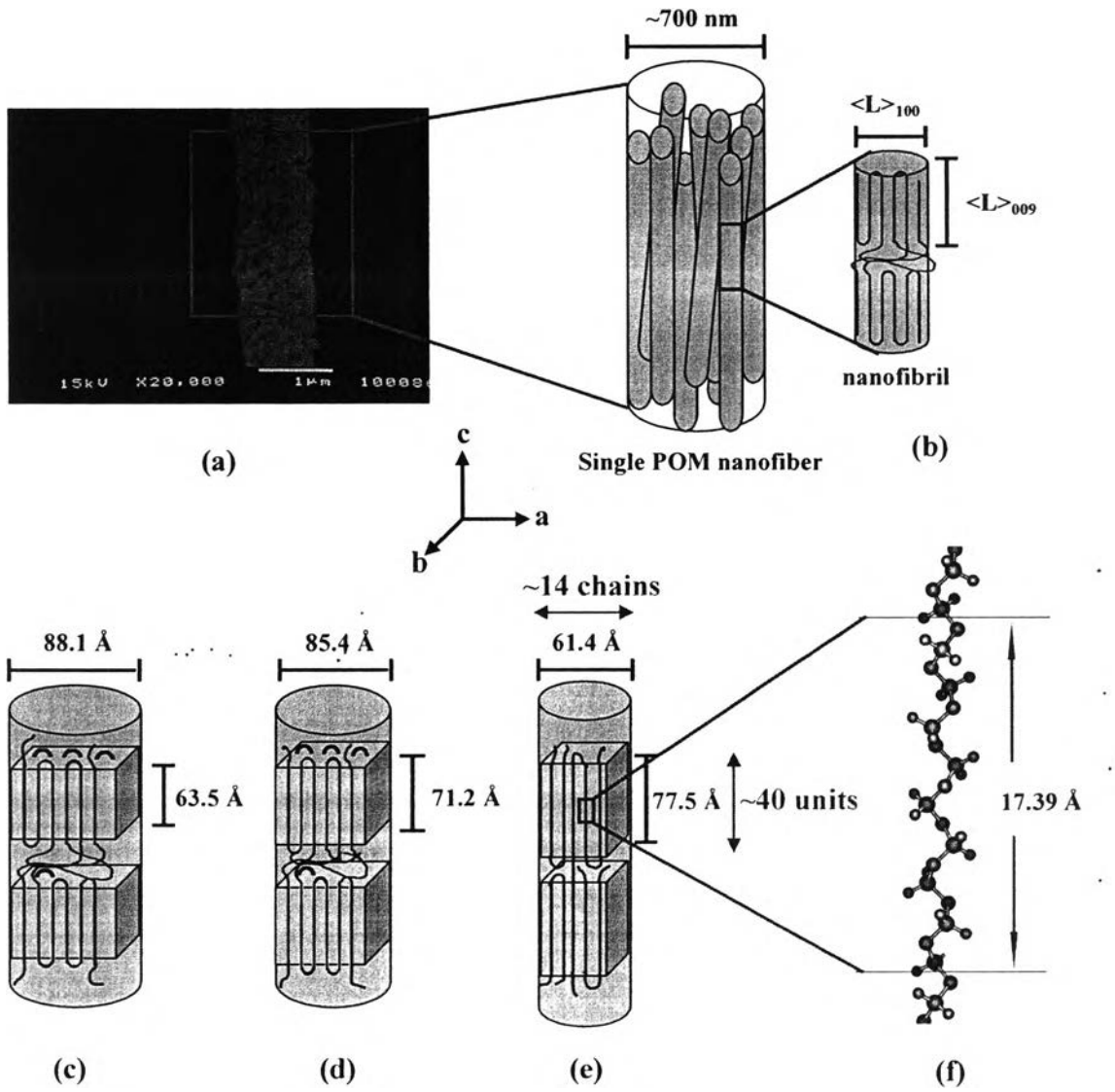

Figure 5.7. (a) SEM micrograph of single POM nanofiber collected at 630 m/min, (b) Schematic representations of nanofibril existed in the single POM nanofiber, (c)–(e) Schematic representations of the crystal orientation of (c) POM at 0 m/min, (d) POM at 630 m/min, and (e) POM at 1890 m/min, (f) Crystal conformation of 9/5 helical structure of the POM chain.

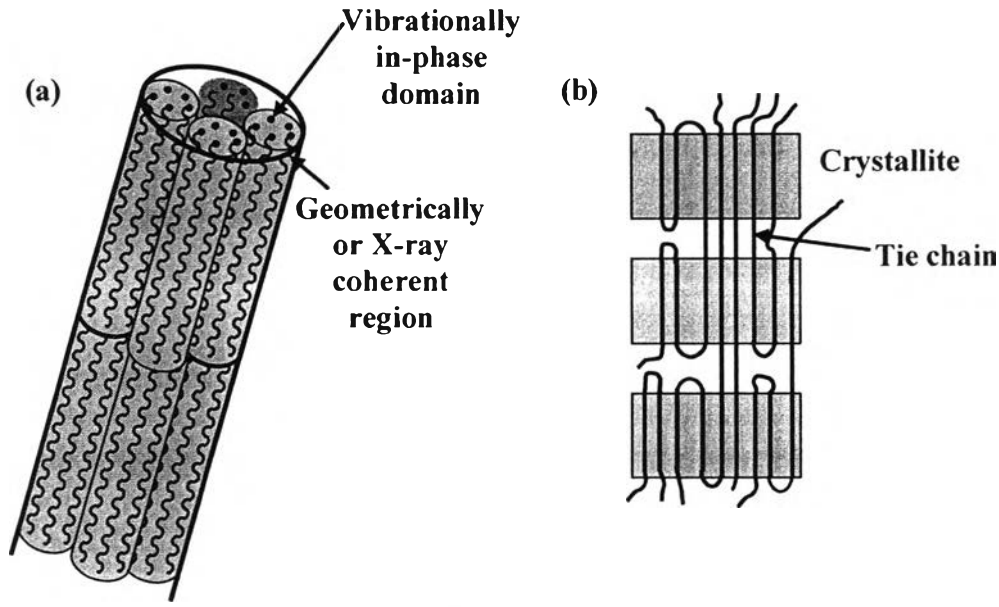

Figure 5.8. Schematic illustration of (a) vibrationally in-phase domain and geometrically-coherent region and (b) existence of tie chains in between the neighboring crystallites.

4. Conclusion

The present work demonstrated a new approach to control crystal morphology and molecular orientation by producing nanofibers via electrospinning process with a rotating disc collector using polyoxymethylene as an example. By controlling the electrical voltage and the rotating velocity of the disc collector, the morphology was changed between an extended chain crystal (ECC) and a folded chain crystal (FCC). Molecular orientation parallel to the fiber axis was observed in both isotropic and anisotropic POM nanofibers. The high rotating disc velocity was not only inducing the ECC morphology but also enhancing the chain to be parallel to the fiber axis. We have been able to clarify the chain aggregation structure in a single nanofiber in which a bundle of nanofibril was recognized. Based on Herman's orientation and crystallite size estimated from the 100 and 009 reflections, it was clear that nanofibril aligned almost

parallel to the fiber axis at the highest rotating speed (1890 m/min) with a bundle of about 14 polymeric chains and ca. 40 monomeric units under 9/5 helical structure.

Acknowledgements. The authors are grateful for the financial support from Mitsubishi Gas Chemical Company, Japan, and Thai Polyacetal Co. Ltd., Thailand. The authors are appreciative for the grant from University Mobility in Asia and the Pacific (UMAP) Program under MOE, Thailand. One of the authors (T.K.) gratefully acknowledges the scholarship from the Petroleum and Petrochemical College, Chulalongkorn University.

References

(1) Jun Zeng, Achim Aigner, Frank Czubayko, Thomas Kissel, Joachim H. Wendorff, Andreas Greiner *Biomacromolecules* **2005;** 6:1484.

(2) Yang, F.; Murugan, R.; Wang, S.; Ramakrishna, S. *Biomaterials* **2005**, *26*, 2603-2610.

(3) Gibson PW, Shreuder-Gibson HL. US Army Soldier and Biological Chemical Command Technical Report Natick/TR-99/016L **1999**.

(4) Gibson PW, Shreuder-Gibson HL, Rivin D. AICHE Journal **1999**;45:190.

(5) Xianyan Wang, Christopher Drew, Soo-Hyoung Lee, Kris J. Senecal, Jayant Kumar, Lynne A. Samuelson *Nano Letters* **2002**;2:1273.

(6) Wang, A.; Singh, H.; Hatton, T. A.; Rutledge, G. C. *Polymer* **2004**, *45*, 5505-5514.

(7) Doshi J., Reneker DH, J Electrostat, **1995**;35:151.

(8) Reneker DH, Yarin AL, Fong H, Koombhongse S. *J. Appl. Phys.* **2000**;87:4531.

(9) Teo, W.E.; Kotaki, M.; Mo, X.M.; Ramakrishna, S. *Nanotechnology* **2005**, 16, 918.

(10) Katta, P.; Alessandro, M.; Ramsier, R.D.; Chase, G.G. *Nano Lett.* **2004**, 4, 2215.

(11) Kameoka, J.; Orth, R.; Yang, Y.; Czaplewski, D.; Mathers, R.; Coates, G. W.; Craighead, H. G. *Nanotechnology* **2003**, *14*, 1124-1129.

(12) Li, D.; Wang, Y.; Xia, Y. *Ad*V. *Mater.* **2004**, *16*, 361-366.

(13) Fennessey, S. F.; Farris, R. J. *Polymer* **2004**, *45*, 4217-4225.

(14) Kakade, M. V.; Givens, S.; Gardner, K.; Lee, K. H.; Chase, D. B.; Rabolt, J. F. *J. Am. Chem. Soc.* **2007**, *129*, 2777-2782.

(15) Tadokoro, H.; Yasumoto, S.; Murahashi, S.; Nitta, I. *J. Polym. Sci.* **1960**, 44, 266.

(16) Carazzolo, G.; *J. Polym. Sci., Part A*, **1960**, 1, 1573.

(17) Kobayashi, M.; Sakashita, M. *J. Chem. Phys.* **1992**, 1, 748.

(18) Bassett, D.C. ; Dammont, F.R. ; Salovey, R. *Polymer* **1964**, 5, 589.

(19) Tadokoro, H.; Kobayashi, M.; Kawaguchi, Y.; Kobayashi, A. ; Murahashi, S. *J. Chem. Phys.* **1963**, 38, 703.

(20) Carter, D.R.; Baer, E.J. *J. Appl. Phys.* **1966**, 37, 4060.

(21) Kobayashi, M.; Sakashita, M. *J. Chem. Phys.* **1992**, 1, 748.

(22) Snetivy D, Vancso GJ, *Macromolecules* **1992**;25:3320.

(23) Kohji Tashiro, Toshiya Kamae, Hitoshi Asanaga, Tetsuo Oikawa. *Macromolecules* **2004**, *37,* 826-830.

(24) J.M. Samon, J.M. Schultz, B.S. Hsiao, S. Khot, H.R. Johnson, *Polymer* **2001** 42:1547–1559.

(25) Iguchi M., *Makromol. Chem.* **1976**;177:549-566.

(26) Shimomura, M.; Iguchi, M. *Polymer* **1982**, 23, 509.

(27) Kobayashi, M.; Morishita, H.; Ishioka, T.; Iguchi, M.; Shimomura, M.; Ikeda, T. *J. Mol. Struct.* **1986**, 146, 155.

(28) Shimomura, M.; Iguchi, M.; Kobayashi, M. *Polymer* **1987**, 29, 351.

(29) Morishita, H.; Kobayashi, M.;Komatsu, T. *Rep. Prog.Polym. Phys. Jpn.* **1987**, 30, 127.

(30) Keller A, Kolnaar HWH. Materials science and technology: a comprehensive treatment, vol. 18. Weinheim: VCH, 1997 (chap. 4, p. 190).

(31) Hama, H; Tashiro, K. *Polymer* **2003**, 44, 3107–3116.